Impact of three-dimensional radiative effects on satellite retrievals of cloud droplet sizes

Alexander Marshak,[1] Steven Platnick,[1] Tamás Várnai,[2] Guoyong Wen,[3] and Robert F. Cahalan[1]

Received 19 September 2005; revised 16 December 2005; accepted 25 January 2006; published 13 May 2006.

[1] There are several dozen papers that study the effects of cloud horizontal inhomogeneity on the retrievals of cloud optical thickness, but only a few of them deal with cloud droplet sizes. This paper is one of the first comprehensive attempts to fill this gap: It takes a close theoretical look at the radiative effects of cloud 3-D structure in retrievals of droplet effective radii. Under some general assumptions, it was found that ignoring subpixel (unresolved) variability produces a negative bias in the retrieved effective radius, while ignoring cloud inhomogeneity at scales larger than a pixel scale (resolved variability), on the contrary, leads to overestimation of the domain average droplet size. The theoretical results are illustrated with examples from Large Eddy Simulations (LES) of cumulus (Cu) and stratocumulus (Sc) cloud fields. The analysis of cloud drop size distributions retrieved from both LES fields confirms that ignoring shadowing in 1-D retrievals results in substantial overestimation of effective radii which is more pronounced for broken Cu than for Sc clouds. Collocated measurements of broken Cu clouds by Moderate Resolution Imaging Spectrometer (MODIS) and Advanced Spaceborne Thermal Emission and Reflection Radiometer (ASTER) are used to check simulations and theory with observations. The analysis of ASTER and MODIS data and associated derived products recommends against blindly using retrieved effective radii for broken cloud fields, especially if one wants to relate aerosol amounts to cloud droplet sizes.

Citation: Marshak, A., S. Platnick, T. Várnai, G. Wen, and R. F. Cahalan (2006), Impact of three-dimensional radiative effects on satellite retrievals of cloud droplet sizes, *J. Geophys. Res.*, *111*, D09207, doi:10.1029/2005JD006686.

1. Introduction

[2] There are several dozen papers that discuss the radiative effects of cloud three-dimensional (3-D) structure on the one-dimensional (1-D) retrievals of cloud optical thickness [e.g., *Marshak et al.*, 1995; *Loeb and Davies*, 1996; *Chambers et al.*, 1997; *Davis et al.*, 1997; *Loeb and Coakley*, 1998; *Zuidema and Evans*, 1998; *Várnai and Marshak*, 2001, 2002a; *Iwabuchi and Hayasaka*, 2002; *Horváth and Davies*, 2004]. Most of these studies assume a "conventional" 10-μm droplet effective radius and variable cloud optical thickness. Though the operational remote sensing of cloud optical properties from multispectral measurements [*Nakajima and King*, 1990; *Platnick et al.*, 2003] typically retrieves cloud optical thickness and effective radius simultaneously, there are only a few papers that, in addition to cloud optical thickness, estimate the effect of cloud inhomogeneity on 1-D retrievals of the droplet effective radius [*Faure et al.*, 2002; *Cornet et al.*, 2004, 2005; *Várnai and Marshak*, 2002b; *Iwabuchi and Hayasaka*, 2003].

[3] Except for Polarization and Directionality of the Earth's Reflectances (POLDER) that retrieves (though not operationally) cloud droplet effective radius from polarization measurements of the reflected light using "cloudbow" (or rainbow) at scattering angles between 150° and 170° [*Deschamps et al.*, 1994; *Bréon and Goloub*, 1998; *Bréon and Doutriaux-Boucher*, 2005], all operational retrievals of cloud droplet size are based on spectral observations [e.g., *Nakajima and King*, 1990]. For the Moderate Resolution Imaging Spectrometer (MODIS), a pair $\{\tau, r_e\}$ that represents cloud optical thickness and droplet effective radius, respectively, is derived for each cloudy 1 km by 1 km pixel from various two band combinations: typically one bulk water-absorption band {1.6, 2.1, or 3.7 μm} and one nonabsorbing (or relatively nonabsorbing) band {0.65, 0.86, or 1.2 μm} [*Platnick et al.*, 2003]. The choice of nonabsorbing band depends on the underlying surface. Since water absorbs differently in the three MODIS absorbing bands, use of the less absorbing 1.6-μm band and the more absorbing 3.7-μm band complement use of the 2.1-μm band for assessing the vertical variation of droplet size in the

[1]NASA Goddard Space Flight Center, Climate and Radiation Branch, Maryland, USA.
[2]Joint Center for Earth System Technology, University of Maryland Baltimore County, Baltimore, Maryland, USA.
[3]Goddard Earth Sciences and Technology Center, University of Maryland Baltimore County, Baltimore, Maryland, USA.

Copyright 2006 by the American Geophysical Union.
0148-0227/06/2005JD006686$09.00

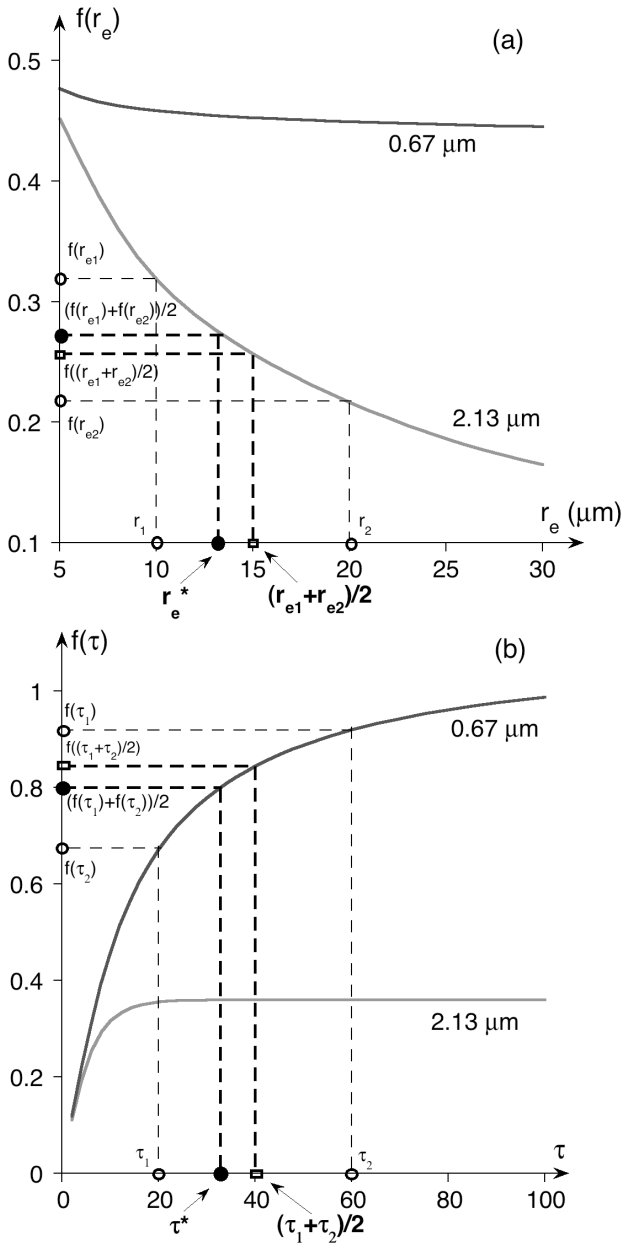

Figure 1. Illustration of the effects of convexity and concavity on averaging. (a) An example of a convex function: nadir reflectances at 0.67 and 2.13 μm versus effective radius, r_e, for r_e between 5 and 30 μm calculated using DISORT. Cloud optical thickness $\tau = 10$. Solar zenith angle $\theta_0 = 41°$; viewing is from nadir, $\theta = 0°$. Surface is absorbing. (b) An example of a concave function: nadir reflectances at 0.67 and 2.13 μm versus optical thickness, τ. Cloud droplet effective radius, $r_e = 10$ μm. Illumination and viewing directions are the same as in Figure 1a; surface is also absorbing. See text for more explanations.

upper portion of the cloud [*Platnick*, 2000; *Platnick et al.*, 2001; *Chang and Li*, 2002].

[4] A growing number of studies on indirect aerosol effects use observed relationships between aerosol amounts and cloud properties such as cloud cover, cloud height and cloud particle size [e.g., *Rosenfeld and Feingold*, 2003; *Kaufman et al.*, 2005; *Koren et al.*, 2005]. For such studies, knowledge of retrieval uncertainty and any possible bias becomes crucial in remote sensing estimates of droplet sizes for different cloud types, especially for broken clouds. The upcoming collection 5 processing stream of the MODIS cloud product operationally provides retrieval uncertainty for both τ and r_e for each cloudy pixel. This uncertainty is derived from the sensitivity of τ and r_e to plane-parallel homogeneous cloud top reflectance, quantified using partial derivatives of τ and r_e with respect to reflectance in both water-absorbing and nonabsorbing bands [*Platnick et al.*, 2005]. The considered (independent) sources of uncertainties are calibration, atmospheric corrections, and surface albedo. The effect of gaseous absorption on uncertainties in water cloud effective radius retrievals is also discussed by *Platnick and Valero* [1995].

[5] The operational MODIS algorithm for retrieval uncertainty (as well as the retrieval algorithm itself) is based on plane-parallel radiative transfer and therefore does not attempt to account for cloud horizontal inhomogeneity. The main purpose of this paper is to complement the 1-D uncertainties by taking a look at the radiative effects of cloud 3-D structure on retrievals of r_e. The outline of the paper is as follows: Section 2 describes the main inequalities that follow directly from "resolved" (at scales larger than a pixel scale) and "unresolved" (at a subpixel scale) cloud horizontal variability. Section 3 analyzes signatures of cloud 3-D structure in the retrieved r_e on the basis of two simulated (stratocumulus and cumulus) cloud fields. An example of cloud retrievals from a broken cumulus cloud over Brazil observed by MODIS is discussed in section 4. Finally, section 5 summarizes the results.

2. Radiative Effects of Resolved and Unresolved Variability

[6] To assess the accuracy of 1-D retrievals one has to distinguish between the radiative effects that are caused by two types of 3-D variability in cloud structure: resolved and unresolved variability. Indeed, 1-D retrievals at a horizontal scale s assume that (1) clouds are horizontally homogeneous at scales smaller than s (unresolved or subpixel variability) and (2) clouds are horizontally homogeneous at scales larger than s (resolved or neighboring pixel variability); that is, the radiation field at a pixel is not influenced by the radiation field of its neighbors. These two assumptions do not overlap and their effects on the accuracy of the retrievals can be quite different. We will study them separately.

2.1. Unresolved Variability

[7] If a functional relationship f between measured quantity y and retrieved value x is monotonic, the effect of ignoring subpixel variability is fully determined (quantitatively) by the type of nonlinearity and (qualitatively) by the degree of nonlinearity. Obviously, if f is linear, simple averaging in x leads to the same averaging in $y = f(x)$, i.e.,

$$f\left(\frac{x_1 + x_2}{2}\right) = \frac{f(x_1) + f(x_2)}{2}. \tag{1a}$$

However, if f is a convex function ($f'' > 0$),

$$f\left(\frac{x_1 + x_2}{2}\right) < \frac{f(x_1) + f(x_2)}{2} \tag{1b}$$

while if f is concave ($f'' < 0$),

$$f\left(\frac{x_1 + x_2}{2}\right) > \frac{f(x_1) + f(x_2)}{2}. \tag{1c}$$

The next two examples illustrate this statement for cloud property retrievals.

[8] Figures 1a and 1b show the well-known dependences of reflectances at two wavelengths: 0.67 μm (conservative nonabsorbing scattering) and 2.13 μm (nonconservative scattering with water absorption) versus effective radius of cloud droplets (Figure 1a) and cloud optical thickness (Figure 1b). We see that function f_r, the relationship between reflectance and effective radius (Figure 1a), is convex while f_τ, the relationship between reflectance and optical thickness (Figure 1b), is concave. Inequalities (1b) and (1c) follow from Figures 1a and 1b, respectively. Note that in both cases, ignoring subpixel variability leads to underestimation of the pixel average retrieved quantity. Indeed, because f_r is a monotonically decreasing convex function, the value r_e* retrieved from the average $\frac{f_r(r_{e1}) + f_r(r_{e2})}{2}$ will be smaller than the pixel average $\frac{r_{e1} + r_{e2}}{2}$. Similarly, because f_τ is a monotonically increasing concave function, it follows from (1c) that the value τ* retrieved from $\frac{f_\tau(\tau_1) + f_\tau(\tau_2)}{2}$ will be smaller than the pixel average $\frac{\tau_1 + \tau_2}{2}$.

[9] To conclude, because of nonlinear relationships between reflectances and cloud optical thickness and effective radius (excluding very small r_e), averaging of reflectances (or ignoring subpixel variability) always results in retrievals that underestimate the true pixel averaged values. The stronger the nonlinearity in the relationship, the larger the underestimation.

2.2. Resolved Variability

[10] Let us consider a cloudy pixel with optical thickness τ and effective radius r_e. Let it be illuminated by the sun at $\Omega_0 = (\theta_0, \varphi_0)$ and viewed at $\Omega = (\theta, \varphi)$ direction. We denote its 1-D plane-parallel reflectance at 0.67 and 2.13 μm wavelengths by $R^{pp}_{0.67}$ and $R^{pp}_{2.13}$, respectively. Now we assume that because of a 3-D cloud structure, instead of $R^{pp}_{0.67}$, we have two categories of measurements $R^{ill}_{0.67} > R^{pp}_{0.67}$ (pixel is "illuminated") and $R^{shad}_{0.67} < R^{pp}_{0.67}$ (pixel is "shadowed"). Similarly, we have two measurements at 2.13 μm: $R^{ill}_{2.13} > R^{pp}_{2.13}$ and $R^{shad}_{2.13} < R^{pp}_{2.13}$. Instead of $\{\tau, r_e\}$, plane-parallel retrievals using the pair of reflectances $\{R^{ill}_{0.67}, R^{ill}_{2.13}\}$ will give $\{\tau + \Delta\tau^{ill}, r_e - \Delta r_e^{ill}\}$ while the pair $\{R^{shad}_{0.67}, R^{shad}_{2.13}\}$ will give $\{\tau - \Delta\tau^{shad}, r_e + \Delta r_e^{shad}\}$ where $\Delta\tau^{ill}$, $\Delta\tau^{shad}$, Δr_e^{ill}, and Δr_e^{shad} are all positive.

[11] Note that calling a pixel "illuminated" ("shadowed") does not necessarily mean here that it receives enhanced (reduced) illumination because it lies on a slope tilted toward (away from) the sun. Rather, a pixel will be called "illuminated" ("shadowed") if, as a result of radiative transfer in the 3-D environment, it reflects more (less) radiation than its plane-parallel counterpart does. Thus a pixel can be called "illuminated" or "shadowed" even for overhead sun.

[12] As a first approximation, we make the following two assumptions that will be examined later: (1) retrievals of τ and r_e are independent, i.e., instead of $\{\tau, r_e\} = f(R^{pp}_{0.67}, R^{pp}_{2.13})$, it is assumed that $\tau = f_{0.67}(R^{pp}_{0.67})$ and $r_e = f_{2.13}(R^{pp}_{2.13})$ where functions $f_{0.67}$ and $f_{2.13}$ map $R^{pp}_{0.67}$ and $R^{pp}_{2.13}$ into τ and r_e, respectively, and (2) plane-parallel reflectance changes from illumination and shadowing are equal for each wavelength, i.e.,

$$R^{ill}_{0.67} - R^{pp}_{0.67} = R^{pp}_{0.67} - R^{shad}_{0.67} = \Delta R_{0.67}, \tag{2a}$$

$$R^{ill}_{2.13} - R^{pp}_{2.13} = R^{pp}_{2.13} - R^{shad}_{2.13} = \Delta R_{2.13}. \tag{2b}$$

What will be the signs of the differences $\Delta\tau^{ill} - \Delta\tau^{shad}$ and $\Delta r_e^{ill} - \Delta r_e^{shad}$ in this case?

[13] Let us start with r_e first. It follows from Figure 1a that $r_e = f_{2.13}(R^{pp}_{2.13})$ is a decreasing convex function at least for $r_e > 5$ μm. Then using inequality (1b), it is easy to see that the average plane-parallel retrieved r_e from equal numbers of illuminated and shadowed pixels with valid equation (2b) is

$$\begin{aligned} r_e &= f_{2.13}\left(R^{pp}_{2.13}\right) \\ &= f_{2.13}\left(\frac{R^{ill}_{2.13} + R^{shad}_{2.13}}{2}\right) < \frac{f_{2.13}\left(R^{ill}_{2.13}\right) + f_{2.13}\left(R^{shad}_{2.13}\right)}{2} \\ &= \frac{r_e^{ill} + r_e^{shad}}{2} = r_e + \frac{\Delta r_e^{shad} - \Delta r_e^{ill}}{2}. \end{aligned} \tag{3}$$

Thus

$$\Delta r_e^{ill} < \Delta r_e^{shad}. \tag{4a}$$

In other words, if a plane-parallel reflectance at 2.13 μm is increased and decreased by the same amount ($\Delta R_{2.13}$), shadowing increases droplet effective radius (makes clouds apparently more absorptive, as stated by *Szczap et al.* [2000]) more than illumination decreases it. Thus the domain averaged effective radius of pixels with the same "true" r_e calculated from equal numbers of illuminated and shadowed pixels is biased high with respect to r_e. Similarly, but for 0.67 μm, using Figure 1b one can show that in contrast to (4a), for optical thickness the inequality is opposite,

$$\Delta\tau^{ill} > \Delta\tau^{shad}; \tag{4b}$$

that is, illumination increases optical thickness more than shadowing decreases it [see *Várnai and Marshak*, 2002a; *Cornet et al.*, 2005]; thus the domain average τ will also be biased high.

[14] To summarize, for a given pixel with optical thickness τ and effective radius r_e, it has been shown that if τ and r_e are retrieved independently and if illumination increases reflectance by the same amount as shadowing decreases it, then the average of illuminated and shadowed pixel optical thickness, $(\tau^{ill} + \tau^{shad})/2$, and effective radius, $(r_e^{ill} + r_e^{shad})/2$, will be larger than their true values. Hence, given the above simplifying assumptions, the resolved variability (or cloud horizontal inhomogeneity at scales larger than the pixel-scale s) will always increase the domain averaged retrieved

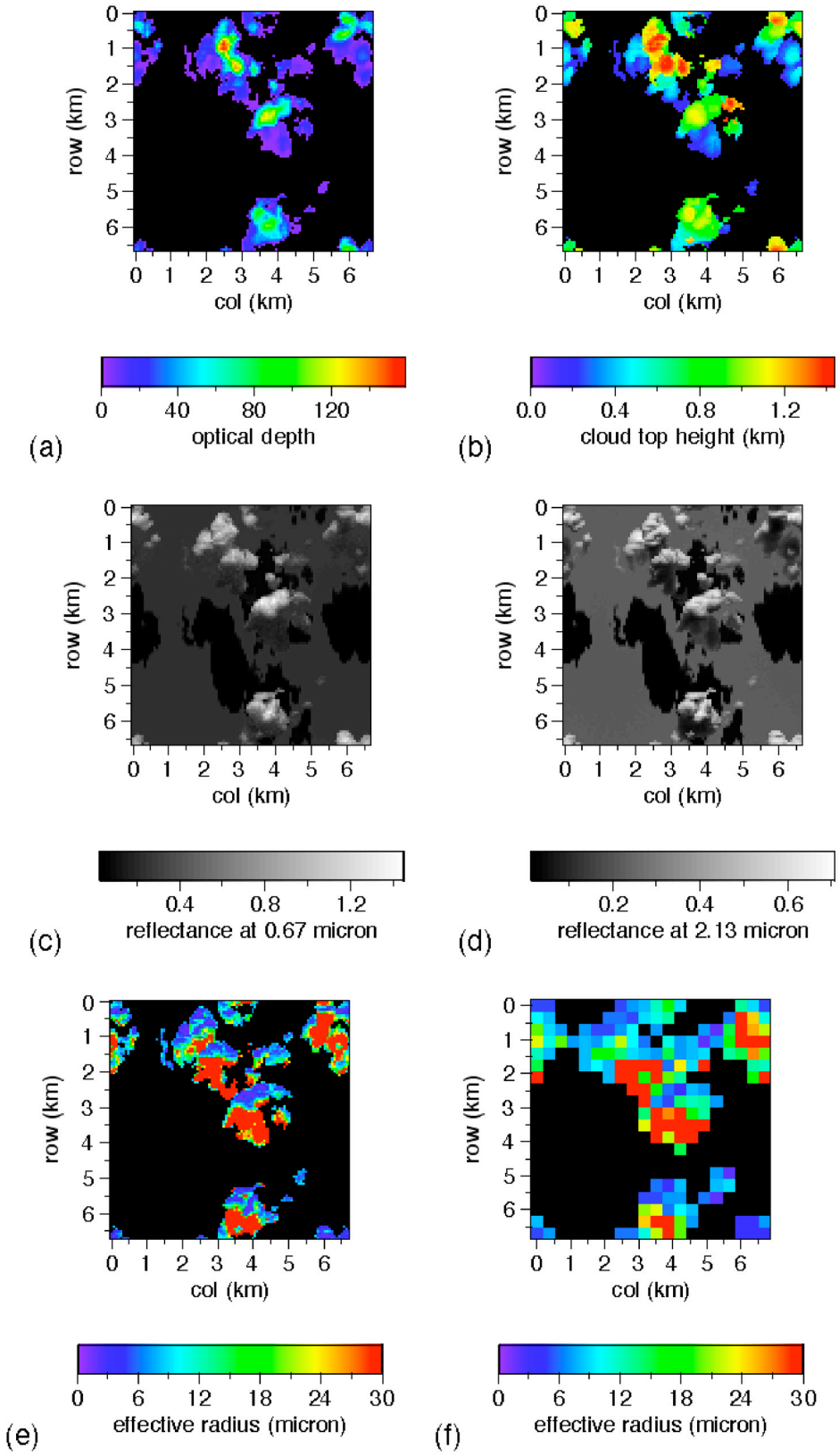
row (km)
col (km)
0 40 80 120
optical depth
(a)
0.0 0.4 0.8 1.2
cloud top height (km)
(b)
0.4 0.8 1.2
reflectance at 0.67 micron
(c)
0.2 0.4 0.6
reflectance at 2.13 micron
(d)
0 6 12 18 24 30
effective radius (micron)
(e)
(f)

Figure 2

optical thickness and droplet effective radius with respect to the values that would be retrieved in a plane-parallel surroundings. Note that this is opposite to the negative bias from subpixel variability discussed in the previous section.

[15] Unfortunately, the last statement has only theoretical value. First, the assumption of independent retrieval of τ and r_e is not generally valid for any values of τ and r_e. However, it can be a reasonable assumption for "large enough" τ and r_e (the exact meaning of "large enough" depends on solar Ω_0 and viewing Ω directions as well as surface brightness, but typically, $r_e > 5$ μm and $\tau > 10$). Second, the assumption that illumination and shadowing change reflectances by the same amount is not valid either; the validity of it strongly depends on solar zenith angle θ_0. It can be shown [e.g., *Davis and Marshak*, 2001] that for high sun, the domain average 3-D reflectance is lower than its 1-D counterpart; hence "shadowing" decreases reflectance more than "illumination" increases it. (Recall that by "shadowing" we understand here not actual shadowing, since there is little shadowing for high sun, but a physical process that reduces reflectance with respect to its plane-parallel counterpart.) The opposite is true for low sun [e.g., *Várnai and Marshak*, 2001].

[16] Thus one can conclude that, on average, for high sun, because of cloud horizontal inhomogeneity, shadowing increases effective radius more than illumination decreases it. In contrast, for low sun, illumination may increase optical thickness more than shadowing decreases it. Similar statements for optical thickness and high sun, and effective radius and low sun, are not necessarily valid, and strongly depend on specific cloud structure and particular solar and viewing angles.

3. Simulation

[17] We will analyze here two Large Eddy Simulation (LES) cloud fields used by the International Intercomparison of 3-D Radiation Codes (I3RC) phase 2 [*Cahalan et al.*, 2005]. The two cloud fields are (1) a cumulus (Cu) cloud field from LES modeling [*Stevens and Lenschow*, 2001] of the GEWEX Cloud System Study continental shallow cumulus boundary layer experiment (the Atmospheric Radiation Measurement (ARM) program Oklahoma site), which consists of 100 × 100 × 36 cells with grid sizes 66.7 m × 66.7 m × 40 m, respectively, and (2) a stratocumulus (Sc) cloud field from LES modeling [*Moeng et al.*, 1996] of FIRE-I stratocumuli, which consists of 64 × 64 × 16 cells with grid sizes 55 m × 55 m × 25 m, respectively. The total horizontal domains are 6.67 km for the Cu case and only 3.52 km for the Sc case.

[18] Figure 2 illustrates the Cu cloud field. Figure 2a shows optical thickness while Figure 2b shows cloud top height. For simplicity, cloud droplet scattering has been described by the Mie phase function with constant effective radius r_e = 10 μm. For solar zenith angle $\theta_0 = 60°$ (illumination from the north, $\varphi_o = 0°$, top of images) and surface albedo of 0.2, nadir bidirectional reflectance fields ($\theta = 0°$) at the nonabsorbing (0.67 μm) and water-absorbing (2.13 μm) wavelengths calculated with a Monte Carlo code are shown in Figures 2c and 2d, respectively.

[19] Let us now assume that cloud optical thickness and effective radius are unknown. Then for each cloudy pixel, they can be inferred from a pair of $\{R_{0.67}, R_{2.13}\}$ reflectances using the *Nakajima and King* [1990] retrieval algorithm. We will focus on the retrieval of r_e comparing retrieved values with the predetermined r_e = 10 μm which we will be calling the "true" value of effective radius.

[20] Figure 2e shows the results of this retrieval. We see that about 30% of all cloudy pixels have a saturated value of r_e = 30 μm. This is the area where $R_{2.13}$ is low (see Figure 2d). Low reflectance at 2.13 μm can result from either (1) small optical thickness, (2) large effective radius, (3) dark surface, (4) 3-D radiative effects, shadowing in particular, or (5) a combination of the above. (Other reasons for low $R_{2.13}$, e.g., a partly cloudy pixel [*Platnick et al.*, 2003] or wrong thermodynamic phase, thus wrong single scattering albedo, are not applicable here for the simulated water clouds.) The average optical thickness, τ, of pixels with a retrieved value of r_e = 30 μm is 24, which is quite large; the true r_e of those pixels is 10 μm, and surface is bright with surface albedo of 0.2. Thus the most likely reason for small $R_{2.13}$ is shadowing. Indeed, a careful analysis of the cloud top height field (Figure 2b) proves a strong correlation between high effective radius and shadowing. In Figure 3 we plotted a 2 km by 1 km region from three fields of Figure 2: nadir reflectance $R_{2.13}$, cloud top height h_t, and retrieved r_e. We clearly see that pixels with high r_e have low cloud height ($h_t \sim 0.3$ km) and are shadowed by the high cloud ($h_t \sim 1$ km) in the upper part of the image. With $\theta_0 = 60°$, the difference in cloud top heights between the northern and southern part of Figure 3 converts into more than 1 km of horizontal cloud surface that does not receive direct solar radiation.

[21] The smallest scale in Figures 2a–2e and Figure 3 is 67 m. Spatial averaging of the measurements improves the retrievals as follows from equation (1b) and section 2.1. Figure 2f shows the retrieved values of r_e when both $R_{0.67}$ and $R_{2.13}$ are averaged over 5 by 5 pixels (335 m) before the retrieval. Indeed, the number of saturated pixels with respect to effective radius decreased from 30% to 18%. Figure 4a illustrates the probability density function of the retrieved r_e for the Cu cloud field and three increasing scales: 67, 134 and 335 m. Because of averaging, the mean r_e decreases from 16.1 to 13.7 μm. This is better illustrated in Figure 4b where mean and standard deviation (std) of the retrieved r_e are plotted for both the Cu and Sc cloud fields. We see that

Figure 2. Cu cloud field and retrieved effective radius. (a) Optical thickness field. (b) Cloud top height field. The cloud is illuminated from the north ($\varphi_0 = 0°$) with a solar zenith angle $\theta_0 = 60°$. Droplet scattering is described by the Mie phase function with constant effective radius r_e = 10 μm. Surface is assumed to be Lambertian with uniform surface albedo 0.2. Rayleigh scattering, molecular absorption and aerosols with vertically varying extinction are used to model the clear atmosphere. (c) Nadir reflectance fields at 0.67 μm calculated by Monte Carlo with 5×10^8 photons. The average simulation error is less than 2%. (d) Same as in Figure 2c but for nadir reflectance at 2.13 μm. (e) Effective radius retrieved from reflectances on Figures 2c and 2d. (f) Same as in Figure 2e but reflectances averaged over 25 pixels.

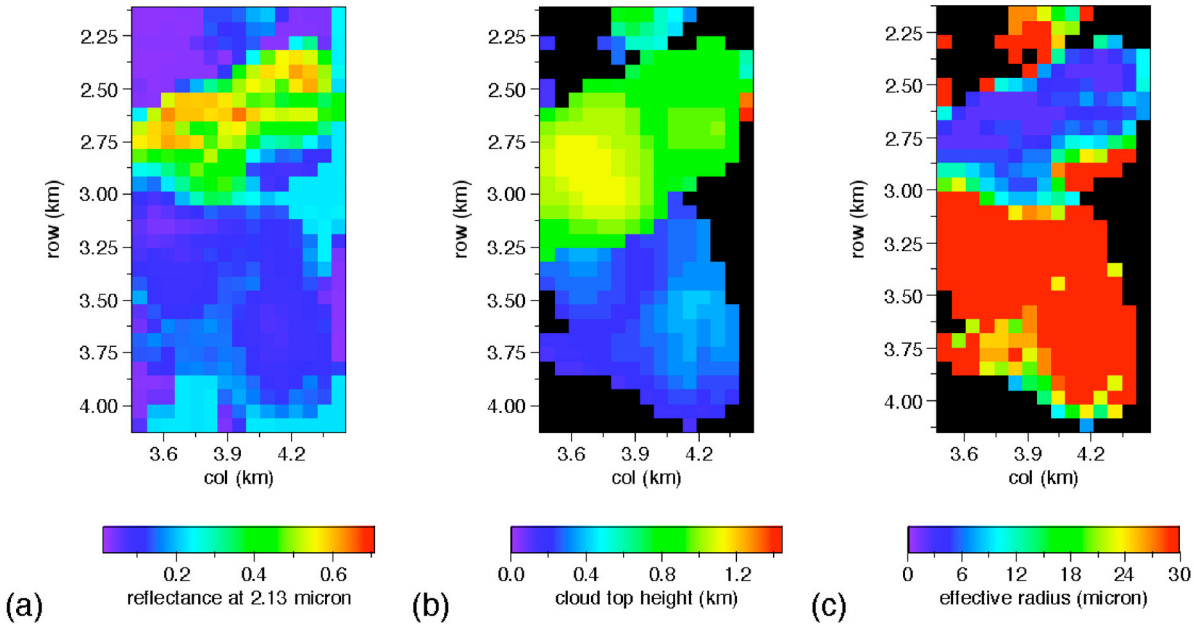

Figure 3. A 2 × 1 km region from Figure 2d (nadir reflectance at 2.13 μm), Figure 2b (cloud top height), and Figure 2e (retrieved r_e).

with averaging, both mean and standard deviation gradually decrease in agreement with the convex nature of the $R_{2.13}$ versus r_e dependence. Note that for the Sc field, because of less shadowing, both the mean and standard deviation of r_e are smaller than those for the Cu field. Also note that here we are talking only about a scale-dependent decreasing of r_e rather than *converging* to the true value (r_e = 10 μm). In the Cu case, r_e > 10 μm even for large scales while for the Sc clouds, the mean r_e goes just below the true value of 10 μm at ∼ 0.9 km. As we see, there are two different physical mechanisms that dominate Cu and Sc scale effects. For Cu, shadowing effects (resolved variability) dominate regardless of scale while for Sc the impact of subpixel (or unresolved) variability becomes dominant after ∼ 1 km. (Recall that operational MODIS retrievals use 1 km pixel observations.) Further averaging does not necessarily improve the retrievals since it leads to so-called plane-parallel biases [*Cahalan*, 1994]. For an example of scale-dependent cloud optical thickness retrievals, see *Davis et al.* [1997, Figure 13].

[22] It is of interest to relate the retrievals of r_e to the retrievals of optical thickness τ. Let us follow *Cornet et al.* [2005] and subdivide all cloudy pixels into two categories based on their retrieved values of cloud optical thickness. Pixels where the true optical thickness, τ_{3D}, is larger than the retrieved optical thickness, τ_{1D}, will be called here "shadowed" while pixels with $\tau_{1D} > \tau_{3D}$ will be called "illuminated." As was pointed out by *Cornet et al.* [2005], the retrieved r_e in the shadowed regions ($\tau_{1D} < \tau_{3D}$) are much larger than the ones in the illuminated ones ($\tau_{1D} > \tau_{3D}$) as if there was more absorption [*Szczap et al.*, 2000; *Cairns et al.*, 2000; *Petty*, 2002]. Using a "r_e versus τ" scatterplot, Figure 5 clearly illustrates this fact for both the Cu and Sc cloud fields.

[23] To summarize, ignoring shadowing in high-resolution 1-D retrieval causes substantial overestimation of r_e for simulated clouds. This effect is much more pronounced for broken Cu than for Sc clouds. Averaging mitigates shadowing, thus decreases the retrieved effective radius for both cloud fields, though for broken Cu averaging over 1–2 km is not necessarily sufficient to avoid pixels with unrealistically high r_e. Finally, overestimation of r_e usually corresponds to underestimation of τ.

4. Observation

[24] To check the above conclusions with observations, we have selected a 1 km spatial resolution MODIS 68 km by 80 km broken Cu cloud scene (Figure 6a) from a less polluted region in Brazil, centered at 17°S and 42°W. The data were acquired on 9 August 2001 at 1015 local time (LT). The solar zenith angle θ_0 = 41°. This scene is part of I3RC phase 3 [*Cahalan et al.*, 2005]. The MODIS image is collocated with a high spatial resolution (15 m) Advanced Spaceborne Thermal Emission and Reflection Radiometer (ASTER) image [*Yamaguchi et al.*, 1998] plotted in Figure 6b. The solar azimuth angle φ_0 = 23° (from upper right corner) as can be confirmed from the casting of the shadows.

[25] Figures 6c and 6d show MODIS band 1 (0.67 μm) and band 7 (2.13 μm) reflectances, respectively. From these two bands MODIS operationally retrieves a 1 km cloud product: cloud optical thickness, τ, and cloud effective radius, r_e [*Platnick et al.*, 2003], plotted in Figures 6e and 6f, respectively. The ratio of cloudy pixels to the total number of pixels gives us the cloud fraction of the scene, which is about 40%. Analyzing the retrieved effective radius, we find that some of the r_e values are very large; one of them even reaches the maximal allowable water cloud retrieval value of r_e = 30 μm. There are 229 pixels with r_e > 25 μm which is 11% of all cloudy pixels (Figure 7a). Figure 7b shows a histogram of cloud optical thickness for pixels with r_e > 25 μm. We see that τ_{mean} = 7.1, τ_{std} = 6.7 and more than

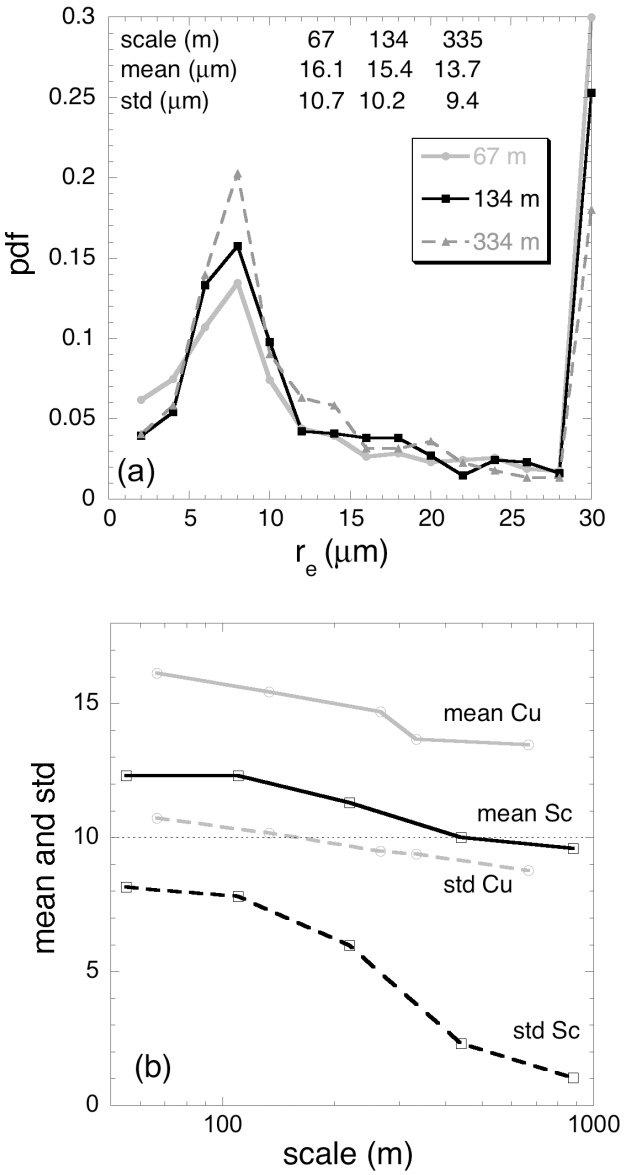

Figure 4. Retrieved effective radius as a function of scale. (a) Probability density function (pdf) of the retrieved r_e for three different averaging scales of the Cu cloud field: 67 m, 134 m and 335 m. (b) Mean and standard deviation (std) of the retrieved r_e versus scale for the Cu and Sc cloud fields. The horizontal dashed line indicates the true r_e = 10 μm.

20% of pixels have optical thickness $\tau > 10$. Let us analyze the image to find out whether these large values of r_e are real or they are caused by the 3-D radiative effects described in the previous sections.

[26] We select a cloudy region from Figure 6 that has a few large retrieved values of r_e. Figure 8 illustrates the 8 × 8 km region highlighted in Figure 6. Figures 8a and 8b represent the 8 × 8 km region of ASTER B3N (nadir, 0.78–0.86 μm) and B14 (10.95–11.65 μm) channels, respectively. The B3N spatial resolution is 15 m while B14 is 90 m. The 8 × 8 km subscenes were cut from ASTER data to match MODIS 8 × 8 km region as best as we could. Figure 8c shows the MODIS retrieved effective radius r_e. In addition, Figures 8d and 8e show cloud top heights for this subscene. A 1 km horizontal resolution cloud top height is not a direct MODIS product (which has 5 km resolution) but can be estimated accurately enough for this scene from measured brightness temperatures. Now we find the locations of pixels with large r_e. Taking into account the solar azimuth of 23° from the top right corner of Figure 8d and from the top of the 3-D Figure 8e, we can conclude that the cloud tops of all pixels with large r_e (>25 μm) are lower than the

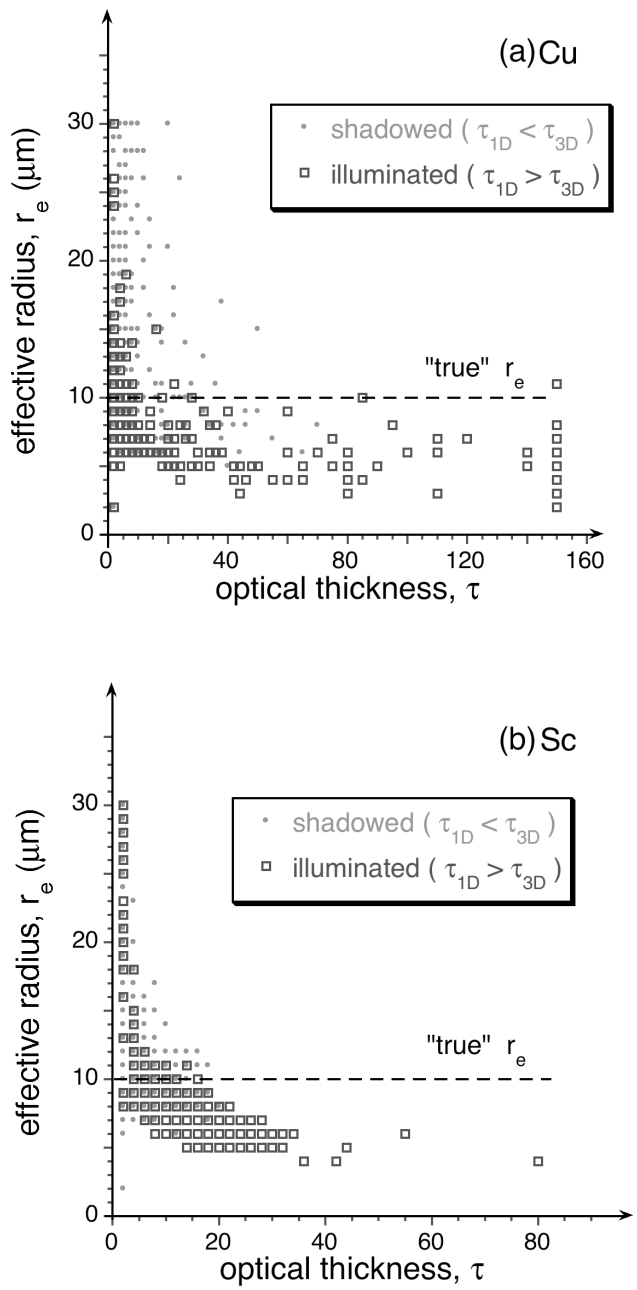

Figure 5. Correlation between retrieved τ and r_e for illuminated and shadowed areas. The horizontal dashed line indicates the true r_e = 10 μm. Note that the maximal allowable retrieval value was set to 150 for optical thickness τ and to 30 μm for effective radius r_e. (a) Cu cloud field for an averaging scale 134 × 134 m. (b) Sc cloud field for an averaging scale 110 × 110 m.

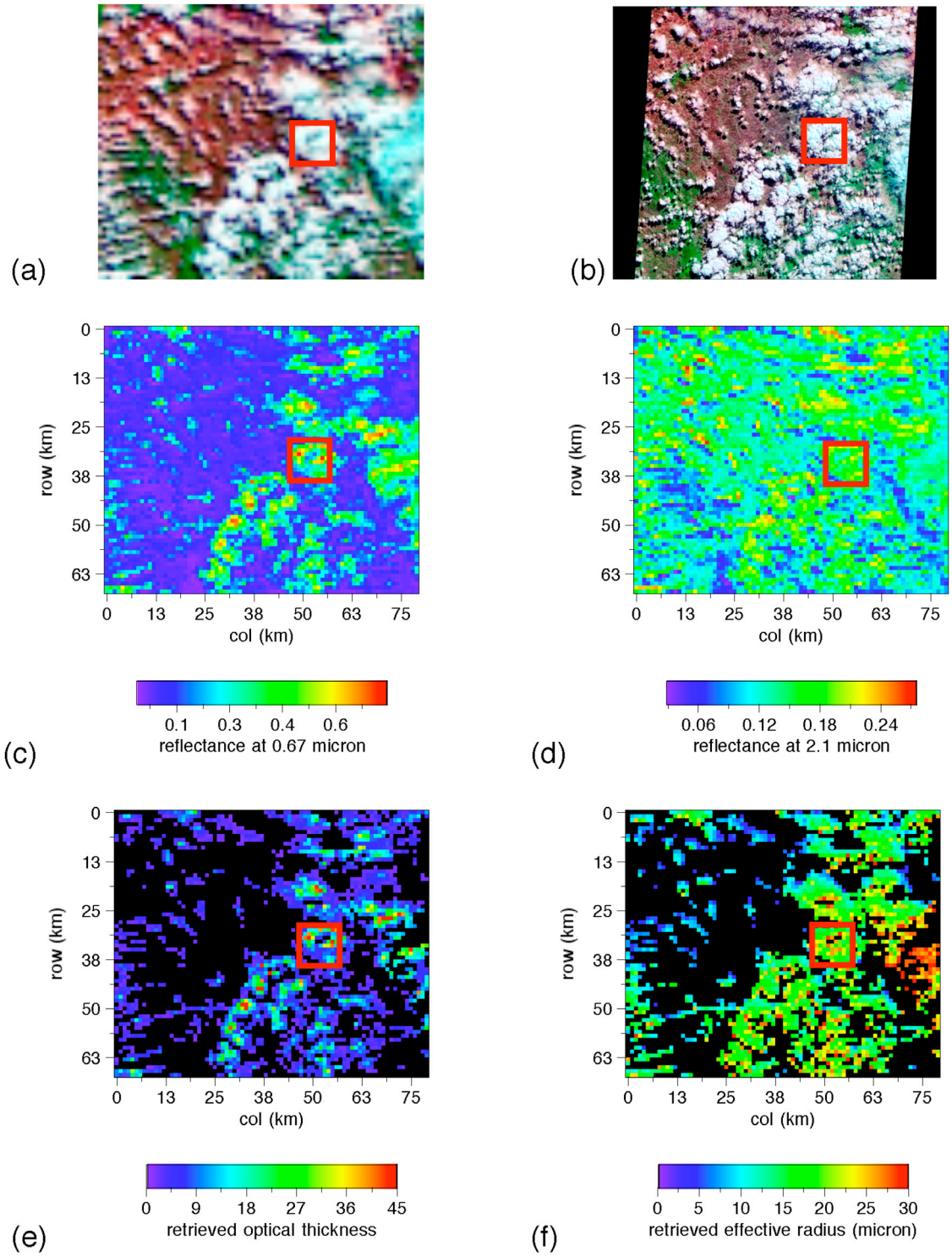

Figure 6. A 68 km by 80 km region in Brazil centered at 17°S and 42°W collected on 9 August 2001 at 1015 LT. The solar zenith angle $\theta_0 = 41°$; the solar azimuth angle $\varphi_0 = 23°$ (from the top). (a) MODIS RGB (2.13, 0.86, 0.47 μm) 1 km resolution, (b) ASTER RGB (2.17, 0.81, 0.55 μm) 15 m resolution, (c) MODIS channel 1 (0.67 μm) reflectance, (d) MODIS channel 7 (2.13 μm) reflectance, (e) retrieved cloud optical thickness, and (f) retrieved effective radius. The (approximate) location of the 8 × 8 km region used in Figure 8 is highlighted.

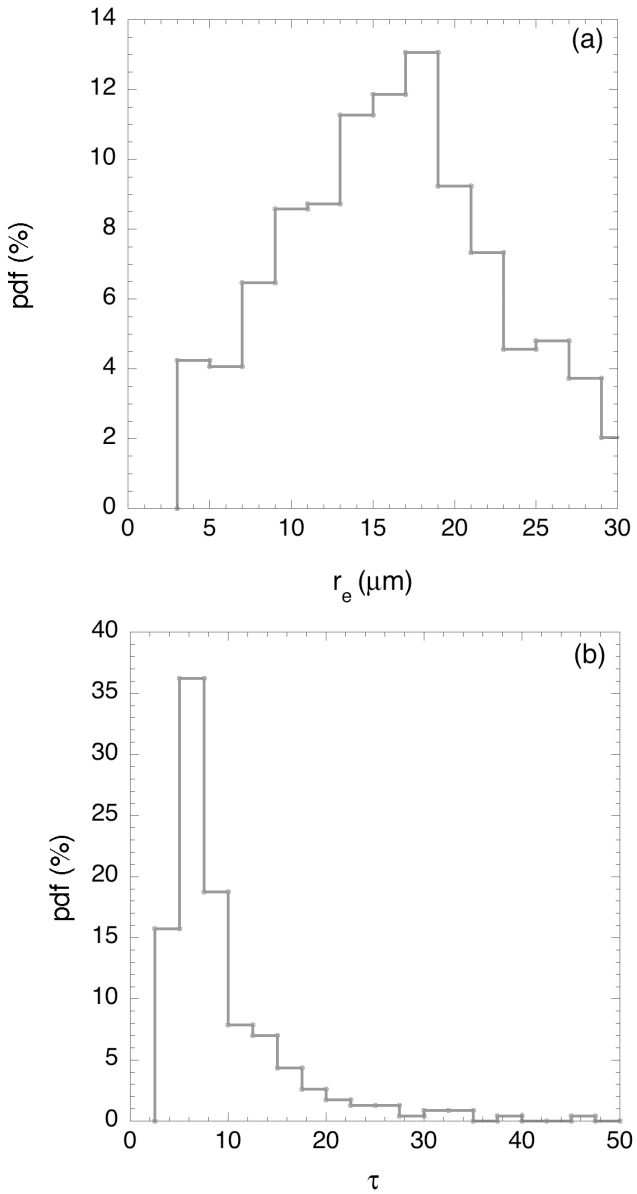

Figure 7. Probability density functions. (a) Retrieved r_e for all cloudy pixels (mean = 16.1, std = 6.4) and (b) retrieved τ for pixels with $r_e > 25$ μm (mean = 7.1, std = 6.7).

cloud tops of their neighboring pixels that lie toward the sun; thus they are in shadow. The same is true for most of the pixels with $r_e > 20$ μm. Therefore their 2.13 μm nadir reflectance is small not because of large highly absorbing droplets but rather because little direct solar radiation can reach those pixels.

[27] Note, that unlike in our simulations, some of the pixels with large effective radii are at cloud edges. These pixels are also likely to be contaminated by clear regions on a subpixel scale [*Platnick et al.*, 2003]. With low surface reflectance (the average diffuse incidence surface albedo at 2.13 μm for pixels with $r_e > 25$ μm is 0.13, and std = 0.02 [see *Moody et al.*, 2005]), the partial cloudiness could contribute to small 2.13 μm nadir reflectances that result in large r_e. However, since the surface reflectance at 0.67 μm is much lower than cloud reflectance (the average surface albedo at 0.67 μm for pixels with $r_e > 25$ μm is 0.06 with std = 0.01), it is unlikely that all pixels with high r_e are contaminated by clear regions. If they were, the retrieved τs could not be as high as the operational retrievals (see histogram in Figure 7b). This is also illustrated in Figure 9 where for all pixels with $r_e > 25$ μm, surface albedos are plotted against nadir reflectances for three MODIS bands (0.67, 1.6, and 2.1 μm). We see that for the 2.1 μm (as well as for 1.6 μm) band more than half of all pixels have a surface albedo larger than the nadir reflectance, which would act to decrease the retrieved droplet effective radius rather than increase it when the surface has sufficient direct illumination.

[28] It is also of interest to analyze pixels with very small r_e, say, $r_e < 5$ μm. There are 4% of those. All of them correspond to small optical thickness with $\tau_{mean} = 2.2$ and $\tau_{std} = 0.6$; droplet size retrievals for these thin cloud have a high uncertainty. The retrieved cloud top height is very low with an average brightness temperature in the 11 μm MODIS band (31) of 294K. It is very likely that some of them are partially cloudy pixels that were misidentified as being overcast.

[29] Another 3-D feature not considered here is the adjacency effect of horizontally inhomogeneous surfaces [*Lyapustin and Kaufman*, 2001]. However, this effect is more pronounced in aerosol remote sensing. With relatively low surface albedos in the 0.67 and 2.13 μm bands, surface inhomogeneity will not have a significant effect on the retrievals of cloud droplet effective radius. The same is true for the validity of the assumption of surface Lambertian reflection versus a bowl shape (bell shape) of its bidirectional reflectance factor (BRF) [*Pinty et al.*, 2005].

[30] We have to admit that among several analyzed MODIS broken cloud scenes, the 3-D effect of shadowing (either geometrical or optical) was not able to explain all large effective radii that had been operationally retrieved. None of other possible reasons we could think of (small cloud optical thickness, subpixel clear sky contamination, wrong thermodynamic phase, multilayered clouds, inhomogeneous surface albedo, absorbing aerosol [see *Haywood et al.*, 2003], or instrumental issues) were able to explain the combination of low 2.13 μm reflectance and relatively high reflectance at 0.67 μm (needed to get a reasonable optical thickness of 10 and higher). In one Amazonian biomass burning scene (acquired on 25 January 2003 and centered at 0°, −53.78° [see *Wen et al.*, 2006]), more than 35% of all cloudy pixels had a retrieved $r_e > 25$ μm; however, they corresponded to low (and homogeneous) 0.67 μm surface albedo (mean = 0.025 and std = 0.04), a retrieved optical thickness of 11±9, and no shadowing geometries. In these cases we cannot think of anything but large droplets to reduce the 2.13 μm nadir reflectance, and thus the retrieval of large r_e appears justified.

[31] To conclude, we found that 3-D shadowing by neighboring pixels toward the sun was responsible for most of the pixels with high retrieved effective radius in broken Cu scenes. In some cases, possible subpixel clear sky contamination and low surface albedo could contribute to low reflectance at 2.13 μm and thus high r_e. However, not all retrieved $r_e > 25$ μm are caused by unaccounted 3-D or

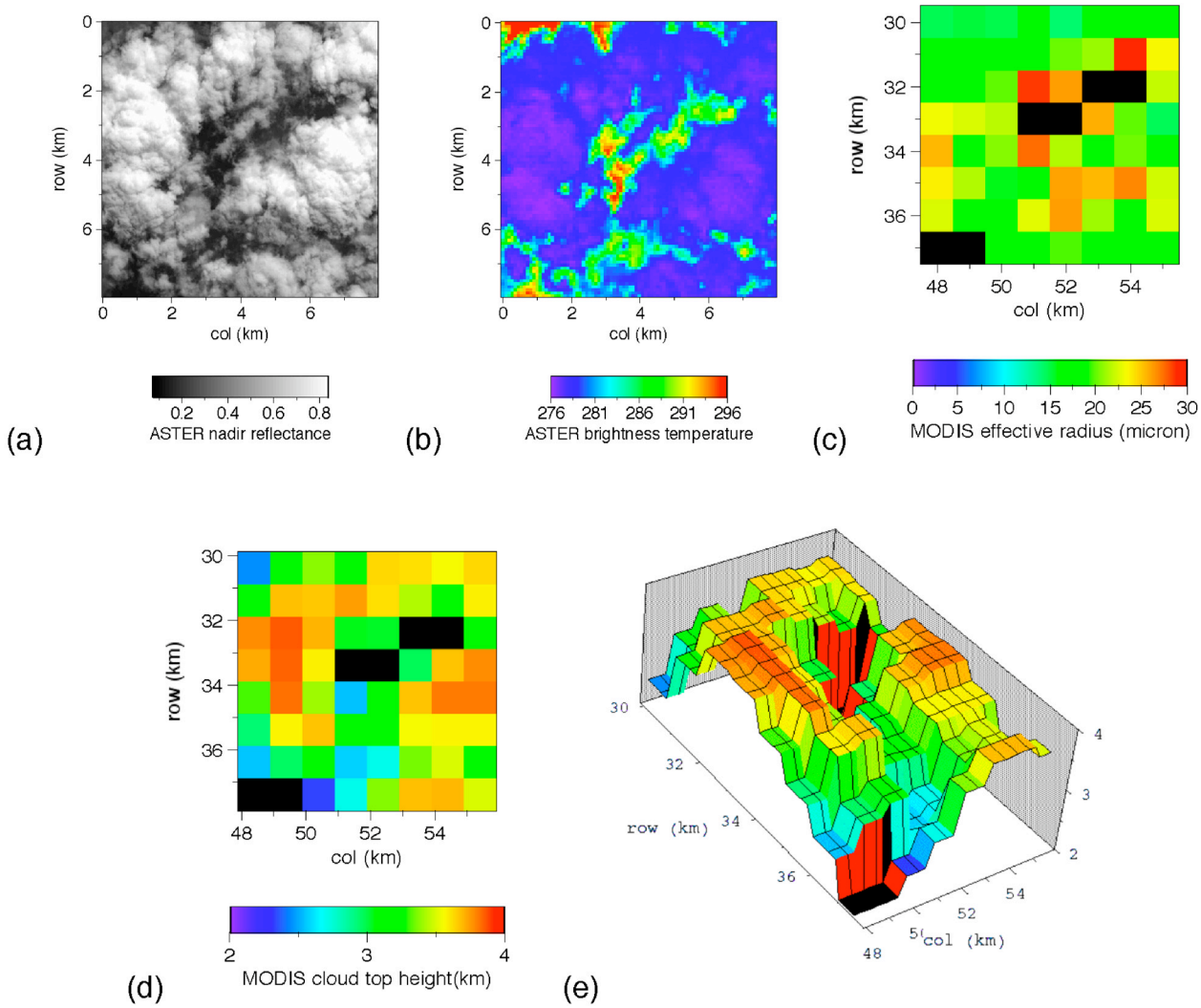

Figure 8. An 8 × 8 km subscene highlighted in Figure 6. (a) 15 m spatial resolution ASTER B3N (nadir at 0.78–0.86 μm); (b) 90 m spatial resolution ASTER B14 (10.95–11.65 μm); (c) MODIS droplet effective radius, r_e, from Figure 6f; (d) MODIS cloud top height, h_t; and (e) same as in Figure 8d but a 3-D height plot. See text for more explanations.

1-D radiative features; in these cases we do not have any reasons to question the retrievals.

5. Summary and Discussion

[32] Two recent papers [*Bréon and Doutriaux-Boucher*, 2005; *Cornet et al.*, 2005] discussed the accuracy of cloud droplet radii retrieved from space. *Bréon and Doutriaux-Boucher* [2005] compared cloud droplet effective radii retrieved from POLDER using the directional signature of the polarized reflectance and from MODIS using spectral signature of cloud reflectance. Though highly correlated over ocean, the two data sets are different by about 2 μm on average, with MODIS showing larger values of r_e. The authors discussed the possible causes for biases including spatial inhomogeneity but were not able to fully explain the 2-μm bias. *Cornet et al.* [2005] used a neural network approach to perform 3-D retrievals of both cloud optical thickness and droplet effective radius and found significant differences between 3-D and operational 1-D retrievals.

[33] In the present paper we used simple theoretical arguments and explicit 3-D computations to understand the influence of 3-D radiative effects on the retrieval of r_e. The main results can be summarized as follows:

[34] 1. Averaging (degrading to larger scales) decreases r_e.

[35] 2. With respect to the plane-parallel approximation, shadowing tends to increase r_e more than illumination decreases it; this results in an overall bias toward larger r_e.

[36] 3. Ignoring shadowing in 1-D retrievals results in substantial overestimation of r_e that often goes in pair with underestimation of τ. This effect is much more pronounced for broken Cu than for Sc clouds.

[37] In addition,

[38] 4. Subpixel clear sky contamination and low surface albedo at 2.13 μm contribute to small nadir reflectance and thus large r_e, and

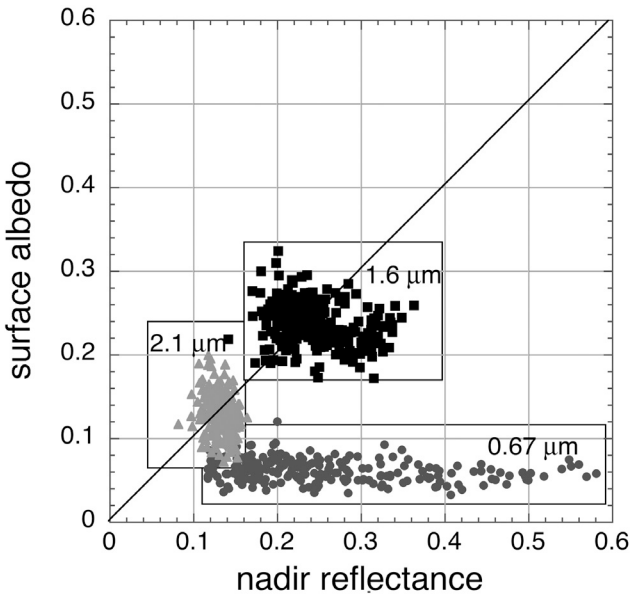

Figure 9. MODIS band-averaged diffuse-incidence surface albedo versus nadir reflectance for pixels with retrieved $r_e > 25$ μm at 0.67, 1.6 and 2.13 μm.

[39] 5. Not all retrieved cloud droplet effective radius $r_e >$ 20–25 μm can be explained by unaccounted 3-D or 1-D radiative features; in these cases, the retrieved large values of r_e could be real.

[40] As retrieval Quality Assessment (QA) parameters, MODIS processing assigns integer numbers from 0 to 3 to each value of retrieved r_e [*Platnick et al.*, 2003]: 0 corresponds to "bad" retrievals, 1 to "marginal," 2 to "good" and, finally, 3 corresponds to "very good" retrievals. Obviously, small optical thickness and large effective radius for water clouds are not very reliable and most likely indicate problems with retrievals that can have 1-D as well as 3-D nature. For example, subpixel broken cloudiness together with low surface reflection and shadowing by the neighboring toward the sun pixels substantially reduces 2.13 μm reflectance, thus giving unrealistically large values of r_e. However, our analysis of Cu Amazonian scenes indicates that not all pixels with large retrieved effective radius are necessarily incorrect. Thus a simple rejection of pixels with large r_e just removes the tail of droplet-size distribution and may introduce a substantial bias.

[41] The upcoming MODIS operational algorithm provides quantitative retrieval uncertainty for all retrievals. Only the uncertainties in surface albedo, atmospheric corrections, and calibration are currently accounted. We are not yet aware of any general recipe that can be operationally applied to Cu broken cloud fields to reject (or correct) unreliable retrievals and keep good retrievals. The decision should be based on a case-by-case study that includes the analysis of the cloud 3-D structure. In order to be confident that there are no biases (in either direction) in the analysis of cloud droplet size distributions, we recommend against blindly using retrieved effective radii for broken cloud fields, especially if one wants to relate aerosol amount to cloud droplet size for studying aerosol indirect effects.

[42] **Acknowledgments.** This work was supported by the Department of Energy (under grant DE-A105-90ER61069 to NASA GSFC) as part of the Atmospheric Radiation Measurement (ARM) program and by NASA Radiation Program Office (under grants 621-30-86 and 622-42-57). We thank Christine Chiu, Anthony Davis, Brian Vant-Hull, Lazaros Oreopoulos, and Warren Wiscombe for stimulating discussions.

References

Bréon, F. M., and M. Doutriaux-Boucher (2005), A comparison of cloud droplet radii measured from space, *IEEE Trans. Geosci. Remote Sens.*, *43*(8), 1796–1805.

Bréon, F. M., and P. Goloub (1998), Cloud droplet effective radius from spaceborne polarization measurements, *Geophys. Res. Lett.*, *25*, 1879–1882.

Cahalan, R. F. (1994), Bounded cascade clouds: Albedo and effective thickness, *Nonlinear Processes Geophys.*, *1*, 156–167.

Cahalan, R. F., et al. (2005), The International Intercomparison of 3D Radiation Codes (I3RC): Bringing together the most advanced radiative transfer tools for cloudy atmospheres, *Bull. Am. Meteorol. Soc.*, *86*, 1275–1293.

Cairns, B., A. A. Lacis, and B. E. Carlson (2000), Absorption within inhomogeneous clouds and its parameterization in general circulation models, *J. Atmos. Sci.*, *57*, 700–714.

Chambers, L., B. Wielicki, and K. F. Evans (1997), On the accuracy of the independent pixel approximation for satellite estimates of oceanic boundary layer cloud optical thickness, *J. Geophys. Res.*, *102*, 1779–1794.

Chang, F.-L., and Z. Li (2002), Estimating the vertical variation of cloud droplet effective radius using multispectral near-infrared satellite measurements, *J. Geophys. Res.*, *107*(D15), 4257, doi:10.1029/2001JD000766.

Cornet, C., H. Isaka, B. Guillemet, and F. Szczap (2004), Neural network retrieval of cloud parameters of inhomogeneous cloud from multispectral and multiscale radiance data: Feasibility study, *J. Geophys. Res.*, *109*, D12203, doi:10.1029/2003JD004186.

Cornet, C., J.-C. Buriez, J. Riedi, H. Isaka, and B. Guillemet (2005), Case study of inhomogeneous cloud parameter retrieval from MODIS data, *Geophys. Res. Lett.*, *32*, L13807, doi:10.1029/2005GL022791.

Davis, A., and A. Marshak (2001), Multiple scattering in clouds: Insights from three-dimensional diffusion theory, *Nucl. Sci. Eng.*, *137*, 251–280.

Davis, A., A. Marshak, R. Cahalan, and W. Wiscombe (1997), The Landsat scale-break in stratocumulus as a three-dimensional radiative transfer effect, implications for cloud remote sensing, *J. Atmos. Sci.*, *54*, 241–260.

Deschamps, P. Y., F. M. Breon, M. Leroy, A. Podaire, A. Bricaud, J.-C. Buriez, and G. Sèze (1994), The POLDER mission—Instrument characteristics and scientific objectives, *IEEE Trans. Geosci. Remote Sens.*, *32*, 598–615.

Faure, T., H. Isaka, and B. Guillemet (2002), Neural network retrieval of cloud parameters from high-resolution multispectral radiometric data. A feasibility study, *Remote Sens. Environ.*, *80*, 285–296.

Haywood, J. M., S. R. Osborne, and S. J. Abel (2003), The effect of overlying aerosol layers on remote sensing retrievals of cloud effective radius and cloud optical depth, *Q. J. R. Meteorol. Soc.*, *130*, 779–800.

Horváth, A., and R. Davies (2004), Anisotropy of water cloud reflectance: A comparison of measurements and 1D theory, *Geophys. Res. Lett.*, *31*, L01102, doi:10.1029/2003GL018386.

Iwabuchi, H., and T. Hayasaka (2002), Effects of cloud horizontal inhomogeneity on the optical thickness retrieved from moderate-resolution satellite data, *J. Atmos. Sci.*, *59*, 2227–2242.

Iwabuchi, H., and T. Hayasaka (2003), A multi-spectral non-local method for retrieval of boundary layer cloud properties from optical remote sensing data, *Remote Sens. Environ.*, *88*, 294–308.

Kaufman, Y. J., I. Koren, L. A. Remer, D. Rosenfeld, and Y. Rudich (2005), The effect of smoke, dust and pollution aerosol on shallow cloud development over the Atlantic Ocean, *Proc. Natl. Acad. Sci. U. S. A.*, *102*(32), 11,207–11,212.

Koren, I., Y. J. Kaufman, D. Rosenfeld, L. A. Remer, and Y. Rudich (2005), Aerosol invigoration and restructuring of Atlantic convective clouds, *Geophys. Res. Lett.*, *32*, L14828, doi:10.1029/2005GL023187.

Loeb, N. G., and J. A. Coakley (1998), Inference of marine stratus cloud optical depths from satellite measurements: Does 1D theory apply?, *J. Clim.*, *11*, 215–233.

Loeb, N. G., and R. Davies (1996), Observational evidence of plane parallel model biases: Apparent dependence of cloud optical depth on solar zenith angle, *J. Geophys. Res.*, *101*, 1621–1634.

Lyapustin, A., and Y. J. Kaufman (2001), Role of adjacency effect in the remote sensing of aerosol, *J. Geophys. Res.*, *106*, 11,909–11,916.

Marshak, A., A. Davis, W. Wiscombe, and G. Titov (1995), The verisimilitude of the independent pixel approximation used in cloud remote sensing, *Remote Sens. Environ.*, *52*, 72–78.

Moeng, C.-H., et al. (1996), Simulation of a stratocumulus-topped planetary boundary layer: Intercomparison among different numerical codes, *Bull. Am. Meteorol. Soc.*, *77*, 261–278.

Moody, E. G., M. D. King, S. Platnick, C. B. Schaaf, and F. Gao (2005), Spatially complete global spectral surface albedos: Value-added datasets derived from Terra MODIS land product, *IEEE Trans. Geosci. Remote Sens.*, *43*, 144–158.

Nakajima, T. Y., and M. D. King (1990), Determination of the optical thickness and effective particle radius of clouds from reflected solar radiation measurements—Part I, Theory, *J. Atmos. Sci.*, *47*, 1878–1893.

Petty, G. (2002), Area-average solar radiative transfer in three-dimensionally inhomogeneous clouds: The independently scattering cloudlet model, *J. Atmos. Sci.*, *59*, 2910–2929.

Pinty, B., A. Lattanzio, J. V. Martonchik, M. M. Verstraete, N. Gobron, M. Taberner, J.-L. Widlowski, R. E. Dickinson, and Y. Govaerts (2005), Coupling diffuse sky radiation and surface albedo, *J. Atmos. Sci.*, *62*, 2580–2591.

Platnick, S. (2000), Vertical photon transport in cloud remote sensing problems, *J. Geophys. Res.*, *105*, 22,919–22,935.

Platnick, S., and F. P. J. Valero (1995), A validation study of a satellite cloud retrieval during ASTEX, *J. Atmos. Sci.*, *52*, 2985–3001.

Platnick, S., J. Y. Li, M. D. King, H. Gerber, and P. V. Hobbs (2001), A solar reflectance method for retrieving the optical thickness and droplet size of liquid water clouds over snow and ice surfaces, *J. Geophys. Res.*, *106*, 15,185–15,199.

Platnick, S., M. D. King, S. A. Ackerman, W. P. Menzel, B. A. Baum, J. C. Riedi, and R. A. Frey (2003), The MODIS cloud products: Algorithms and examples from Terra, *IEEE Trans. Geosci. Remote Sens.*, *41*(2), 459–473.

Platnick, S., R. Pincus, B. Wind, M. D. King, M. Gray, and P. Hubanks (2005), An initial analysis of the pixel-level uncertainties in global MODIS cloud optical thickness and effective particle size retrievals, *SPIE Proc.*, *5652*(2), 1–12.

Rosenfeld, D., and G. Feingold (2003), Explanation of discrepancies among satellite observations of the aerosol indirect effect, *Geophys. Res. Lett.*, *30*(14), 1776, doi:10.1029/2003GL017684.

Stevens, B., and D. H. Lenschow (2001), Observations, experiments, and large eddy simulations, *Bull. Am. Meteorol. Soc.*, *82*, 283–294.

Szczap, F., H. Isaka, M. Saute, B. Guillemet, and A. Ioltukhovski (2000), Effective radiative properties of bounded cascade absorbing clouds: Definition of effective single scattering albedo, *J. Geophys. Res.*, *105*, 20,635–20,648.

Várnai, T., and A. Marshak (2001), Statistical analysis of the uncertainties in cloud optical depth retrievals caused by three-dimensional radiative effects, *J. Atmos. Sci.*, *58*, 1540–1548.

Várnai, T., and A. Marshak (2002a), Observations and analysis of three-dimensional radiative effects that influence MODIS cloud optical thickness retrievals, *J. Atmos. Sci.*, *59*, 1607–1618.

Várnai, T., and A. Marshak (2002b), Observations of three-dimensional radiative effects that influence satellite retrievals of cloud properties, *Idojaras*, *106*, 265–278.

Wen, G., A. Marshak, and R. F. Cahalan (2006), Impact of 3D clouds on clear sky reflectance and aerosol retrievals in biomass burning region of Brazil, *Geosci. Remote Sens. Lett.*, *3*, 169–172.

Yamaguchi, Y., A. B. Kahle, H. Tsu, T. Kawakami, and M. Pniel (1998), Overview of Advanced Spaceborne Thermal Emission and Reflection Radiometer (ASTER), *IEEE Trans. Geosci. Remote Sens.*, *36*, 1062–1071.

Zuidema, P., and K. F. Evans (1998), On the validity of the independent pixel approximation for the boundary layer clouds observed during ASTEX, *J. Geophys. Res.*, *103*, 6059–6074.

R. F. Cahalan, A. Marshak, and S. Platnick, Climate and Radiation Branch, NASA Goddard Space Flight Center, MD 20771, USA. (alexander.marshak@nasa.gov)

T. Várnai, Joint Center for Earth System Technology, University of Maryland Baltimore County, Baltimore, MD 21250, USA.

G. Wen, Goddard Earth Sciences and Technology Center, University of Maryland Baltimore County, Baltimore, MD 21250, USA.